Electrostatic potential of mean force between two curved surfaces in the presence of counterion connectivity

Shiqi Zhou*

School of Physics and Electronics, Central South University, Changsha, Hunan 410083, China

(Received 17 July 2015; revised manuscript received 26 September 2015; published 30 November 2015)

In this paper, we investigate effects of counterion connectivity (i.e., association of the counterions into a chain molecule) on the electrostatic potential of mean force (EPMF) between two similarly charged cylinder rods in a primitive model electrolyte solution by solving a classical density functional theory. The main findings include the following: (i) The counterion connectivity helps in inducing a like-charge-attractionlike (LCA-like) phenomenology even in a monovalent counterion solution wherein the LCA-like observation generally does not occur without the counterion connectivity. (ii) For divalent counterion solutions, the counterion connectivity can reinforce or weaken the LCA-like observation depending on the chain length N, and simply increases the equilibrium nearest surface separation of the rods corresponding to the minimum EPMF to nearly three times the counterion site diameter, whether N is large or small. (iii) If N is large enough, the LCA-like strength tends to be negatively correlated with the electrolyte concentration c over the entire range of the rod surface charge magnitude $|\sigma^*|$ considered; whereas if N drops, the correlation tends to become positive with decrease of the $|\sigma^*|$ value, and particularly for modest $|\sigma^*|$ values, the correlation relationship exhibits an extreme value phenomenon. (iv) In the case of a 1:1 electrolyte, the EPMF effects of the diameters of counterion and coion sites are similar in both situations with and without the counterion connectivity. All of these findings can be explained self-consistently by a recently proposed hydrogen-bonding style mechanism reinforced by one additional concept: flexibility of the counterion chain and the factors affecting it, like N and counterion site valence.

DOI: 10.1103/PhysRevE.92.052317 PACS number(s): 64.70.pv

I. INTRODUCTION

Many liquid systems of interest have two or more chemical components. In many cases, however, only a subset of these components can be observed directly in a given experimental setup, and the presence of other components can only be indirectly perceived by their influences on the ''observable'' components. In static light scattering or videomicroscopy experiments on colloidal systems, for example, it is usually the case that only the static structure of the colloidal particles themselves is detected, and the correlations among the remaining components (salt ions, water molecules, polymers, etc.) are usually invisible to these techniques. Equilibrium microstructures measured in this type of experiment can be determined by using an effective pair potential (EPP) also called a potential of mean force (PMF) among the observable particles that reproduces their pair correlations. From a theoretical point of view, the EPP [1–3] can be obtained from a "contraction" of the description of multicomponent systems, and the presence of the nonobservable components is then taken into account through their influences on the EPP. Depletion interaction is a kind of EPP and, consequently, understanding the depletion potential between colloidal components due to the presence of various nonadsorbing species provides a basis for manipulation of colloidal dispersion microstructures, phase behaviors, stability, and the resulting material properties (e.g., rheology, optical properties) [4–10].

The depletion effect has been extensively studied in the area of colloid-polymer mixtures, where small neutral polymers induce depletion interactions between large colloidal particles. Adsorption of polymers from solution to solid surfaces is usually used to control interfacial properties such as steric stabilization or flocculation, surface tension, and lubrication properties [11–14]. This is especially important in many practical applications including cosmetics, water treatment, foodstuffs, paint, and inks, in which application of solid particles often involves a use of polymers. Polymers may be physically adsorbed or chemically attached to the colloid surfaces, or free in bulk solution. Whatever forms the polymers take, their presence will significantly mediate the interaction between two surfaces. A large body of research shows that, at low concentrations of depleting agents, large colloidal particles experience only an effective attraction; at higher concentrations, however, the colloid pair potential also has a repulsive barrier due to structuring of the depleting agents within the gap. The forces between two particles in a solution depend mainly on whether the polymer is attracted (adsorbed) to or repelled (depleted) from the particle surface. On the one hand, addition of nonadsorbing polymers to the colloid suspension can result in so-called polymer-mediated "depletion attraction" between particle pairs; on the other hand, an attachment of polymers to the two surfaces by grafting or strong adsorption is a common method of stabilizing large particles in a solution [15,16]. When a colloidal particle approaches another one, the two attached polymer layers begin to overlap, and limited interpenetration of chains in good solvents leads to effective repulsion and to a steric stabilization of the colloids. For mixtures of charged colloid particles and uncharged polymer coils, there is a competition between the long-range electrostatic repulsion and the short-range entropic depletion attraction. For these systems, the colloid structure goes from electrostatically stabilized colloidal clusters to the formation of attractive gels [17–20]. In recent years, attention has been driven to colloid-polymer mixtures where

*chixiayzsq@yahoo.com

the two species are like charged, and for this particular case, the effective depletion attraction between the two colloids becomes greatly enhanced by the colloid-polymer electrostatic repulsion. For charged colloid-polymer mixtures where the colloid and polymer are differently charged, the effective depletion interactions will definitely present different traits. On the other hand, when the Van der Waals force (called the dispersion force) among the depleting particles is taken into account, distribution of the depleting particles within the gap between two large objects is bound to change, and the corresponding depletion interaction between the large objects also changes accordingly by presenting a deviation with respect to the hard sphere depletion potential. Nevertheless, because of the coupled chain connectivity and long-range electrostatic interaction, polyelectrolyte depletants have received much less attention, particularly in theoretical studies, as compared to the conventional neutral polymers and simple electrolytes. Consequently, the understanding of the polyelectrolyte depleting behavior is rather incomplete.

A description of electrostatics in solution will inevitably concern the role of electrical double layers (EDLs). Standard textbook theories of the EDL are based on a Poisson-Boltzmann (PB) theory, a mean-field theory that describes a system in terms of the mean electrostatic potential and the average concentration of the mobile ions. At large surface-charge magnitude, high counterion valency, and high ion concentration—the so-called strong-coupling limit, the PB theory fails to capture a number of qualitative effects observed in experiments and simulations, such as like-charge attraction [21–24] and charge inversion [25,26]. In this regime, an Ornstein-Zernike integral equation method [27–29] and a strong-coupling theory [30–32] have been employed to account for the strong interionic correlations. Under weak-coupling conditions, it is generally accepted that the EDL is well described by the PB theory. However, a number of phenomena involving the EDL under the weak-coupling conditions, such as the long-range electrostatic attraction between two neutral plates [33], the slow ion transport in the ion channels [34], and salt effects on bubble coalescence in water [35], cannot be explained, even qualitatively, by the PB theory. A method even better than the PB theory, the Ornstein-Zernike integral equation method, and the strong-coupling theory is the so-called classical density functional theory (DFT) [36], which retrieves the effects omitted in the PB theory. A large number of studies show that the classical DFT is remarkably successful in dealing with interfacial phenomena and structure [37–43]; Recent work [44] has shown conclusively that a traditional density functional approximation for the EDL consisting of a simple electrolyte solution at a charged surface, as will be sketched below, is surprisingly accurate even under strong-coupling conditions characterized by considerable asymmetries in ion valence and size, and extremely high ion molar concentration.

The aim of the present paper is twofold. One of the goals is to obtain knowledge of the modification of the electrostatic potential of mean force (EPMF) in the presence of a polyelectrolyte that is differently charged by comparison with the colloid surface charges, by probing a wide parameter range. Another goal is to explore the validity of a hydrogen-bonding style mechanism (HBSM) [23,24], originally proposed for a salt-ion-induced LCA, in the polyelectrolyte problem, and extend its application range beyond the salt ions by introducing additional concepts characterizing the charged chain molecule. It is noted that typically the LCA refers to an attraction generated by correlations between ions on purely electrostatic grounds. In contrast, the attractions found in the present paper and in the literature [23,24] are due to the competition of the electrostatic interaction, hard-core repulsion, and conformational entropy ("connectivity"); such an interplay of the electrostatic and nonelectrostatic interactions does not qualify to be called LCA. Consequently, we use the word "LCA-like" to denote the attraction found in the present paper; moreover, the proper expression for the attractions found in the literature [23,24] also should be "LCA-like." The rest of this paper is organized as follows: In Sec. II, a brief review of the DFT approach used is presented and then applied to calculate the EPMF occurring between two similarly charged rods immersed in a polyelectrolyte water solution. In Sec. III, the calculated EPMF results are presented, and their main features are described and compared with those originating from the simple electrolyte solution instead of the present polyelectrolyte water solution; based on the comparisons, we analyze the role of counterion connectivity in the EPMF between two similarly charged rods, and formulate a self-consistent explanation for the polyelectrolyte-induced EPMF. Finally, in Sec. IV, we summarize the present findings and formulate perspectives and future developments of the model.

II. METHOD

The subject of the present study is similar to that in Ref. [23] except that the counterions (here, cations) are tangentially bonded together to form a freely jointed and positively charged chain [45], and the counterions constituting the chain have the same valence. The polyelectrolyte solution making up the bath, with which the EDL around the two similarly and negatively charged cylinder rods is in equilibrium, consists of fluid mixtures of positively charged chains and negatively charged coions dissociated from the chains. As regards the role of anion connectivity in the EPMF, for length reason it will be discussed independently in a separate presentation. A primitive model (PM) is used for the polyelectrolyte solution, where the solvent is implicitly described by its dielectric constant, and interactions among the counterion sites forming the chain and the coions are given by a summation of hard-sphere interaction and Coulombic interaction, as described in the literature [44]. For simplicity, the cylinder rod and solution have the same dielectric constant. The Helmholtz free energy functional $F[\{\rho_\alpha\}]$ describing the present system is comprised of an ideal gas contribution and an excess contribution $F_{\rm ex}$, viz.,

$$F[\{\rho_\alpha\}] = k_B T \sum_\alpha \int d\mathbf{r}\rho_\alpha(\mathbf{r})\left\{\ln\left[\rho_\alpha(\mathbf{r})\lambda_\alpha^2\right] - 1\right\} + F_{\rm ex}[\{\rho_\alpha\}], \quad (1)$$

where λ_α is the thermal de Broglie wavelength of the αth component, k_B is the Boltzmann constant, and T is the absolute temperature. The excess contribution $F_{\rm ex}$ originates

from internal interactions within the system, and is in general unknown. For the present system consisting of positively charged chains and anions; it is comprised of $F_{\text{short\_hr}}$, due to the short-ranged hard-sphere interactions appearing when the counterion sites and coions approach each other closely, F_{Coul}, due to a direct Coulombic interaction among the counterion sites and coions, F_{coupling}, due to coupling of the Coulombic and hard-sphere interactions, and $F_{\text{ex,assoc}}$ due to association of the counterion sites in the chain:

$$F_{\text{ex}}[\{\rho_\alpha\}] = F_{\text{short\_hr}}[\{\rho_\alpha\}] + F_{\text{Coul}}[\{\rho_\alpha\}] + F_{\text{coupling}}[\{\rho_\alpha\}] + F_{\text{ex,assoc}}[\{\rho_\alpha\}]. \quad (2)$$

The first three terms and the final term $F_{\text{ex,assoc}}$ in Eq. (2) are dealt with as described in the literature [44] and according to the description in Ref. [45], respectively, and repeated briefly here because of the essential importance in reproducing the results.

$F_{\text{short\_hr}}[\{\rho_\alpha\}]$ is dealt with by an enhanced Kierlik-Rosinberg (KR) third-order equation of state (EOS) [46] which incorporates a recent third-order expansion equation of state [47] into a Kierlik-Rosinberg version [48] of an original Rosenfeld fundamental measure functional (FMF) [49]. It is indicated [46] that the high accuracy and self-consistency of the third-order EOS confirms the KR-FMF third-order EOS proper for rather severe state conditions.

F_{Coul} is given in the mean field approximation as

$$F_{\text{Coul}}[\{\rho_\alpha\}] = \frac{1}{2}\sum_{\alpha\beta}\int d\mathbf{r} \times \int d\mathbf{r}'\rho_\alpha(\mathbf{r})\rho_\beta(\mathbf{r}')u_{\text{Coul\_}\alpha\beta}(|\mathbf{r}-\mathbf{r}'|), \quad (2a)$$

where $u_{\text{Coul\_}\alpha\beta}(r)$ denotes the potential due to direct Coulombic interactions among salt ions and is given by

$$u_{\text{Coul\_}\alpha\beta}(r) = \begin{cases} 0, & r < d_{\alpha\beta}, \\ q_\alpha q_\beta / r\varepsilon, & r > d_{\alpha\beta}, \end{cases} \quad (2b)$$

where q_α is the electric charge of the α component in units of coulombs, and $\varepsilon = \varepsilon_0\varepsilon_r$ is the permittivity of the solution with ε_0 the vacuum permittivity and ε_r the relative permittivity of the solution medium.

A second-order functional perturbation expansion approximation is employed to deal with F_{coupling}:

$$F_{\text{coupling}}[\{\rho_\alpha\}] = F_{\text{coupling}}\left[\{\rho_\alpha^b\}\right] + \int d\mathbf{r}\sum_\alpha - k_BT\Delta c_\alpha^{(1)\text{coupling}}\left[\rho_\alpha(\mathbf{r}) - \rho_\alpha^b\right] + (1/2)\iint d\mathbf{r}d\mathbf{r}'\sum_\alpha\sum_\beta - k_BT\Delta c_{\alpha\beta}^{(2)\text{coupling}}(|\mathbf{r}-\mathbf{r}'|) \times \left[\rho_\alpha(\mathbf{r}) - \rho_\alpha^b\right]\left[\rho_\beta(\mathbf{r}') - \rho_\beta^b\right], \quad (2c)$$

where $\Delta c_\alpha^{(1)\text{coupling}}$ and $\Delta c_{\alpha\beta}^{(2)\text{coupling}}(r)$ are the coupling parts of the bulk first- and second-order direct correlation functions (DCFs), respectively, and $\Delta c_{\alpha\beta}^{(2)\text{coupling}}(r)$ is obtainable in the following way:

$$\Delta c_{\alpha\beta}^{(2)\text{coupling}}(r) = c_{\alpha\beta}^{(2)}(r) + \beta u_{\text{Coul\_}\alpha\beta}(r) - c_{\text{HS\_}\alpha\beta}^{(2)}(r), \quad (2d)$$

where the bulk second-order DCF $c_{\alpha\beta}^{(2)}(r)$ is for an overall neutral mixture of charged hard spheres, i.e., the bulk electrolyte solution in the PM, and is analytically available in the form of the mean spherical approximation [50]. $\Delta c_\alpha^{(1)\text{coupling}}$ is obtained by functional integration of $\Delta c_{\alpha\beta}^{(2)\text{coupling}}(r)$, and $F_{\text{coupling}}[\{\rho_\alpha^b\}]$ is obtainable via the fluctuation route and the expression for $\Delta c_{\alpha\beta}^{(2)\text{coupling}}(r)$.

$F_{\text{ex,assoc}}[\{\rho_\alpha\}]$ is treated by a modified interfacial statistical associating fluid theory (MISAFT) [45], which applies broadly to a range of inhomogeneous complex fluids, giving the exact density profile for ideal chains in an external field; when the MISAFT is applied to lipids near surfaces, lipid bilayers, and copolymer thin films, the theoretical results show excellent agreement with molecular simulations.

It may be worth explaining the meaning of the mean field approximation. If an approximation for the Helmholtz free energy gives a bulk second-order direct correlation function in the form of β times the negative potential function, then the approximation is called the mean field approximation. As a result, in the present paper, the direct Coulombic interaction is treated by the mean field approximation, whereas the hard-sphere interaction and hard-sphere-Coulombic interaction are dealt with by a non-mean-field approximation.

In the classical DFT, one works in the grand canonical ensemble and the corresponding grand potential $\Omega[\{\rho_\alpha\}]$ is related to the intrinsic Helmholtz free energy $F[\{\rho_\alpha\}]$ via a Legendre transform:

$$\Omega[\{\rho_\alpha\}] = F[\{\rho_\alpha\}] + \sum_\alpha\int d\mathbf{r}\rho_\alpha(\mathbf{r})[u_\alpha(\mathbf{r}) - \mu_\alpha], \quad (3)$$

where μ_α is the chemical potential of the αth component, and $u_\alpha(\mathbf{r})$ is an external potential, acting on the αth component, which consists of an electrostatic part due to the presence of external charges such as the charges smeared on two cylinder rods in this paper, and a nonelectrostatic part due to a confining geometry or combination of several confining geometries, such as the two cylinder rods standing face to face of the present interest. In the present calculations, the nonelectrostatic term is hard, i.e., it disappears when the ion surface loses contact with the rod surface and is infinite otherwise; whereas the electrostatic term is treated in the same way as in the literature [23]. After minimization of the grand potential $\Omega[\{\rho_\alpha\}]$, the equilibrium single-particle density distribution $\{\rho_\alpha\}$ is obtained and is used further to obtain the grand potential itself by substituting $\{\rho_\alpha\}$ into the expression for $\Omega[\{\rho_\alpha\}]$. From the calculated grand potential and density distributions, one can easily acquire all the other relevant thermodynamic quantities such as the EPMF as a function of the rod nearest surface separation h, a central theme of this study. The two negatively charged cylinder rods considered are hard, and do not exert a dispersion force on the counterion sites and coions. In the text, the asterisk marks a reduced quantity; more specifically, one uses $d = 4.2$ Å as the unit of length, and, correspondingly, the counterion and coion reduced densities ρ_+^* and ρ_-^*, respectively, are defined as $\rho_\pm d^3$; the nearest rod surface separation h and cylinder diameter d_{cylinder} are reduced

as $h^* = h/d$ and $d^*_{\text{cylinder}} = d_{\text{cylinder}}/d$, respectively; the surface charge density σ of the rod is reduced as $\sigma^* = \sigma d^2/e$ (e is the electron charge in units of coulombs); the reduced excess grand potential per unit surface area in units of k_BT is reduced as $\Omega^*_{\text{ex}} = \Omega_{\text{ex}} d^2/k_BT$, and $\Omega_{\text{ex}} = \Omega - \Omega^b$ is easily calculated by importing the equilibrium density distributions and bulk densities into the grand potential expression. Some parameters are fixed throughout the calculations unless otherwise stated; they are $T = 298$ K, the relative permittivity of the solution medium $\varepsilon_r = 78.5$, and $d^*_{\text{cylinder}} = 5$.

According to the definition, the reduced EPMF per unit area and in units of k_BT is calculated as

$$u^*_{\text{elec}}(h) = \Omega^*_{\text{ex}}(h) - \Omega^*_{\text{ex}}(h_{\max}), \tag{4}$$

where $h_{\max}$ is large enough that $u^*_{\text{elec}}(h)$ will no longer change when $h_{\max}$ increases progressively. It should be noted that as the reported EPMF u^*_{elec} is measured per unit surface area and in units of k_BT, the EPMF per unit rod length should be equal to $u^*_{\text{elec}} \pi d_{\text{cylinder}} k_BT$. As a result, as one will see subsequently, the EPMFs per unit rod length reported in the present sample calculations is most often around k_BT, so they are physically meaningful.

The validity of the disparate elements of the free energy functional $F[\{\rho_\alpha\}]$ of present interest has been confirmed. On the one hand, the sum of $F_{\text{short\_hr}}[\{\rho_\alpha\}]$, $F_{\text{Coul}}[\{\rho_\alpha\}]$, and $F_{\text{coupling}}[\{\rho_\alpha\}]$ constitutes the excess free energy functional of the simple PM electrolyte, and has been illustrated [44] to be accurate even under quite harsh conditions, such as considerable asymmetries in ion valence and size, extremely high ion molar concentration; on the other hand, the validity of $F_{\text{ex,assoc}}[\{\rho_\alpha\}]$ has also been confirmed [45] in the presence of intersegment hard-sphere interaction and attraction interaction to model lipids near surfaces, lipid bilayers, and copolymer thin films. Consequently, Eq. (2) can be reasonably expected to work for electrolyte systems with ions connected into a chain molecule.

III. RESULTS AND DISCUSSION

In the present work, we concentrate on the influences of counterion connectivity on the EPMF between two similarly charged cylinder rods. In addition to the site number or length N of the counterion chain, we will also calculate the effects of different combinations of N and other electrolyte solution parameters, as these effects on the EPMF in different cases will supply necessary clues for exploring the relevant mechanism causing the effects. Throughout the paper, an $c:m$ electrolyte means that the cations making up the chain have valence n, and the dissociated anions have valence m.

The present results for the EPMF are presented in Figs. 2–7, and we will discuss these results one by one in relation to three-dimensional counter- and coion density profiles for several representative situations, as documented in Figs. 8–11. By comparing the present Figs. 3–6 and the figures displayed in Refs. [23,24], one knows that the EPMF curves are far more kaleidoscopic in the presence of counterion connectivity than in the absence of the counterion connectivity. Consequently, neither the equilibrium nearest surface separation h^*_e (corresponding to the lowest point of the EPMF curve) nor the LCA-like strength will provide enough descriptions of the EPMF curves in various parameter combinations. As the EPMF curves in the presence of counterion connectivity are rarely reported, full views of the EPMF curves in various parameter combinations will give valuable information. So the EPMF curves in various parameter combinations are documented.

The following analysis will show that our discoveries can best be explained with the help of the HBSM [23,24] recently proposed for dealing with the EPMF between two spherical or cylindrical surfaces on which some quantity of charges are evenly smeared. By appealing to fairly common-sense concepts such as bond energy, bond length, the number of hydrogen bonds formed, and the counterion single-layer saturation adsorption capacity, the HBSM successfully explains many EPMF observations based on experiments, simulations, and theoretical calculations. Reinforced by the two concepts of the counterion effective adsorption spaces belonging to different localized surface charges and the hydrogen bond directivity, the HBSM is further advanced to successfully explain the effects of discreteness of surface charges on the EPMF [42]. Below, we will exemplify the application of the HBSM to the effects of counterion connectivity on the EPMF.

According to the HBSM [23,24,42] the LCA-like strength is positively correlated with the energy and number of "hydrogen bonds" created. Of the two quantities, the hydrogen bond energy is positively related to the valence of the counterion playing the role of the hydrogen atom in the case of the negatively charged surface of the present interest, and negatively related to the bond length, which is the sum of lengths I and II. With regard to the bond length of the hydrogen bond, there needs to be a further explanation. Figure 1 shows the lengths I and II, and the so-called surface subdomains involved in the hydrogen bond creation, and it is clearly shown that the length I measures the separation between some surface subdomain of one of the two negatively charged surfaces taking the role of the oxygen atom (hydrogen donor) of a water molecule and an adsorbed counterion playing the role of the hydrogen atom of the same water molecule; and length II measures the separation between the adsorbed counterion and the empty surface domain of the other of the two negatively charged surfaces which is not covered by the counterion and serves as the oxygen atom (hydrogen acceptor) of the other water molecule involved in the hydrogen bonding. In addition, the

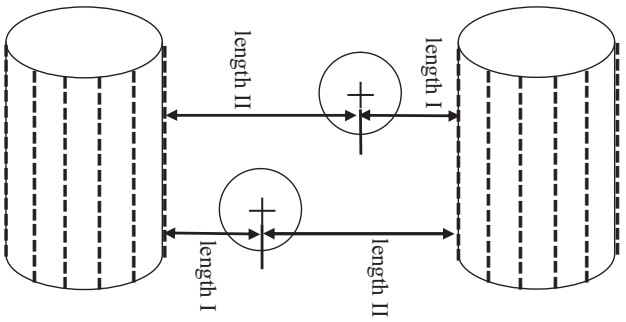

FIG. 1. Diagram of the HBSM for explaining the EPMF between two similarly charged cylinder rods immersed in an electrolyte solution.

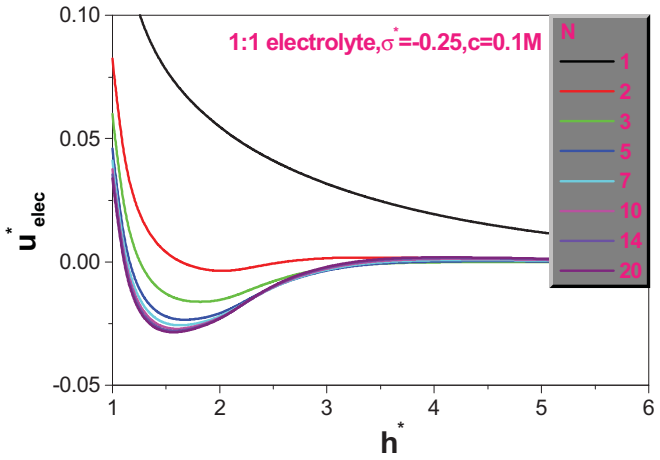

FIG. 2. (Color online) Effect on the EPMF of site number N of the counterion chain. Values of other solution parameters considered are noted in the figure and described in the text.

hydrogen bond energy is positively related to magnitude of surface charges contributing to the actual formation of the hydrogen bond and playing the role of the oxygen atoms (hydrogen donor and hydrogen acceptor, respectively) of the two water molecules involved in the hydrogen bonding. The number of hydrogen bonds created is determined by the counterion single-layer adsorption capacity, which is limited by the counterion single-layer saturation adsorption capacity, which determines the maximum number of hydrogen bonds likely to be formed, and obviously negatively related to the counterion size, and positively correlated with the counterion effective adsorption space (a concept used in the case of the discrete surface charges [42]). However, it should be noticed that the actual counterion single-layer adsorption also depends on the adsorption force field, which is obviously positively correlated with the surface charge magnitude and counterion valence, and negatively related to the temperature and relative permittivity of the solution medium. In addition, when the hydrogen bond directivity is violated, then the hydrogen bond energy will drop. In Fig. 1 the length II is deliberately shown to be longer than the length I, and this is because continuing reduction of the length II will necessarily cause the two counterions to be in close proximity and consequently an increase of the system energy level. As a result, the continuing reduction of the length II is forbidden. On the other hand, although an increase of the perpendicular distance between two counterions helps in weakening the continually increasing direct electrostatic repulsion between the two counterions with the dropping of the length II, and allows the length II to be reduced further to a certain extent, the counterion adsorption capacity's decrease accompanying the increasing of the perpendicular distance reduces the number of hydrogen bonds likely to be created, and also raises the system energy level; as a result, a thinner counterion layer is also forbidden. In brief, the lengths I and II are determined by many factors, and the bond length or the final equilibrium distance is a rigorous statement of the principle of the grand potential minimum, which also corresponds to the equilibrium density profile.

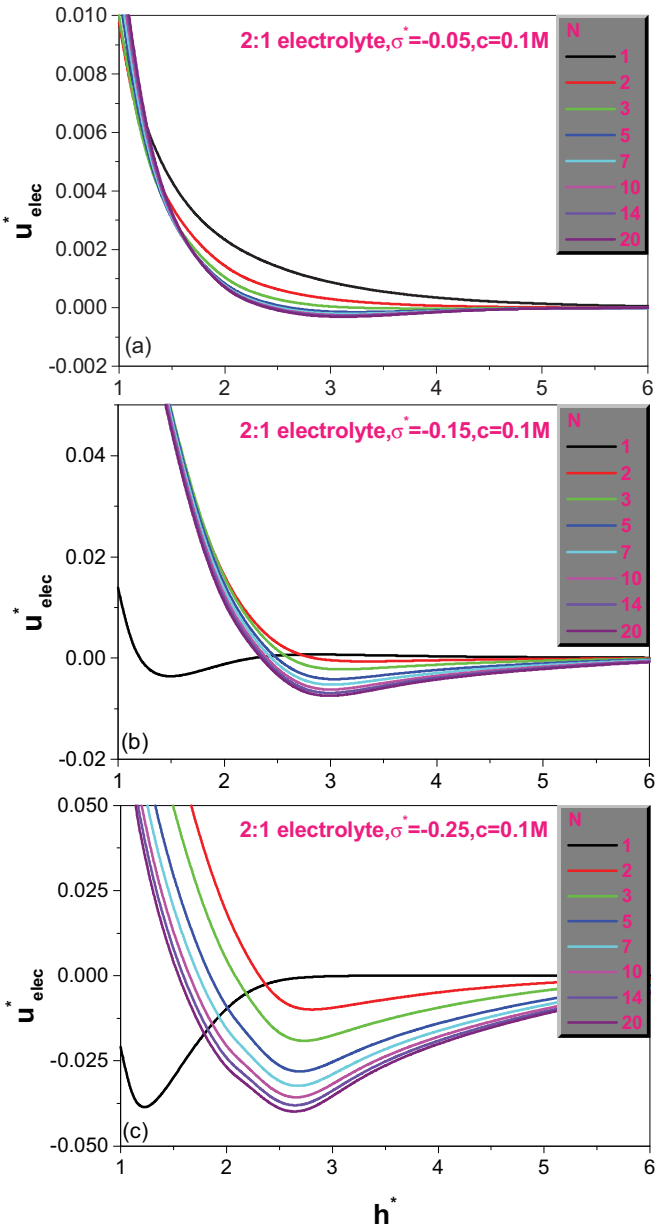

FIG. 3. (Color online) As Fig. 2 except that the effect of the surface charge density is also considered as well as that of the site number N of the counterion chain. The 2:1 type electrolyte is considered.

It is known that the LCA-like will not materialize in the 1:1 simple electrolyte solution if the bulk electrolyte concentration and colloid surface charge strength are not high enough, as literature [23,24] shows. From Fig. 2, one notices that the counterion connectivity helps in inducing the LCA-like observation even in a 1:1 simple electrolyte solution in which originally there is no LCA-like phenomenon. Concretely speaking, the longer the counterion chain, the more obvious the inductive effect; however, the inductive effect tends to become stable as the site number N of the counterion chain reaches approximately 20. In the meantime, the equilibrium nearest surface separation h_e^* is reduced with increase of N and becomes almost constant when N is more than 20. It is known

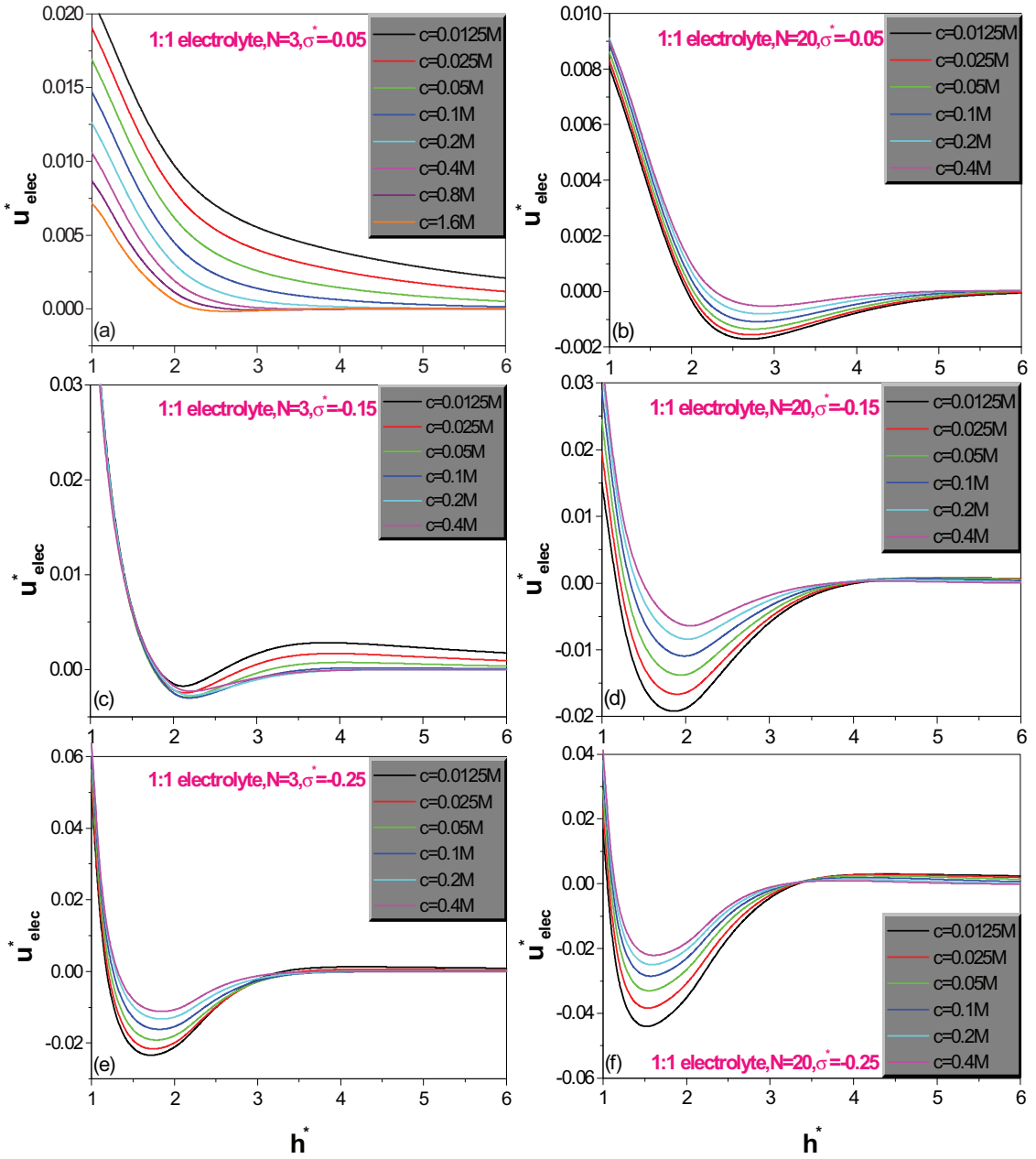

FIG. 4. (Color online) Effect on the EPMF of electrolyte molar concentration c subjected to different combinations of site number N of the counterion chain and surface charge density σ^*. The 1:1 type electrolyte is considered.

that decreasing of h_e^* with increase of the LCA-like strength accords with the fact that hydrogen bonding energy varies inversely with the bond length [23,24]. Unlike Fig. 2 wherein the 1:1 type electrolyte is considered, in Fig. 3 we investigate the N effect in a 2:1 type electrolyte solution, and three values of the reduced surface charge density σ^* are considered. The information Fig. 3 conveys includes the following: (i) When the σ^* value is low enough even the divalent counterion ($N = 1$) fails to elicit the LCA-like behavior, and this has been explained quite successfully by means of the HBSM [23,24]. (ii) Although the counterion connectivity is a plus factor in causing the LCA-like phenomenon, its eventual occurrence depends on the extent to which the contributing factors have been at work. Specifically, in the case of Fig. 3(a) wherein $|\sigma^*| = 0.05$ is relatively low, $N = 2$ is insufficient to generate the LCA, and $N = 3$ and beyond is necessary to induce the LCA. Moreover, the LCA-like strength is always very low. (iii) As represented in Fig. 2 for the case of a 1:1 electrolyte, the same N effect rule is also true for the 2:1 electrolyte, i.e., a longer counterion chain will induce the LCA-like phenomenon more strongly, and the positive correlation effect becomes stable as N reaches 20; moreover, h_e^* is also reduced with the increase of N for the interval with $N \geqslant 2$. (iv) An additional observation emerging from Fig. 3 is that when the value of $|\sigma^*|$ is high enough so that the LCA-like behavior arises in the 2:1 simple electrolyte solution, the counterion connectivity clearly causes h_e^* to be elevated to nearly 3 and to be larger than 2; whereas under similar conditions h_e^* is usually less than

1.5 times the counterion diameter without the presence of the counterion connectivity.

As regards the inductive effect of the counterion connectivity, we think that it is due to an increase of the magnitude of charges carried by the near surface counterion chain as a complete entity in comparison with the case in the absence of the counterion connectivity. As it is the near surface counterion chain which plays the role of the hydrogen atom in the hydrogen bond formation, an increase of the excess positive charge magnitude of the hydrogen atom would entail a stronger hydrogen bond. To support the above guess, three-dimensional density profiles of the total counterion site and coion are displayed in Fig. 8 for the two cases of Fig. 2 and in Fig. 9 for the two cases of Fig. 3(c). It is shown that the maximum near surface total reduced counterion site density ρ_+^* certainly increases in Fig. 8 from approximately 1.155 for $N = 1$ to 1.385 for $N = 20$, and in Fig. 9 from approximately 1.635 for $N = 1$ to 2.53 for $N = 3$. However, the less obvious increase of ρ_+^* in Fig. 8 seems not enough to alone explain the very evident increase of the LCA-like strength with the N value, as documented in Fig. 2; there should be other coexisting reasons responsible for the obvious LCA-like strength-N correlation. Figures 8 and 9 show that in comparison with the nearly complete depletion of the coions from the near surface domain in $N = 1$, there is a considerable amount of coion aggregation between the two rod surfaces for $N = 3$ and 20. Considering the attractive interaction between the counter- and coions, the coion aggregation between the two rod surface domains, initially populated exclusively by the counterions in the $N = 1$ case, will certainly reduce the osmotic pressure between the two rod surfaces. It is thought that it is the combined variation of the hydrogen bond energy and osmotic pressure that induces the observed change of the LCA-like strength with the N value.

However, the above explanation leads to a new problem remaining to be solved, i.e., how to explain the saturation phenomenon for the LCA-like strength and h_e^* with the site number N? When N progressively increases, the flexibility of the chain also increases accordingly, and the counterion chain can adopt a conformation which causes the sites to be arranged along the rod surface so that h_e^* approaches the corresponding value in the simple electrolyte solution. Compared to the simple ion without connectivity, the number of configurations the chain can adopt is eventually constrained by the connectivity, and as a result h_e^* with the counterion connectivity will be always larger than h_e^* in the simple electrolyte, as demonstrated in all of the figures, which show that h_e^* in the presence of the counterion connectivity generally exceeds 1.5 times the counterion site diameter, whereas h_e^* is usually less than 1.5 times the counterion diameter without the presence of the counterion connectivity. One may wonder why h_e^* is larger in the 2:1 electrolyte than in the 1:1 electrolyte? On the one hand, it is logical that for the same N, the chain comprised of divalent counterion sites will be less flexible than that consisting of univalent counterion sites as the electrostatic repulsion is stronger for the divalent case than for univalent case, and the electrostatic repulsion serves to keep the occupied sites as far away from each other as possible; on the other hand, it is easy to understand that the less flexible the chain, the more difficult it is for the chain to adopt conformations

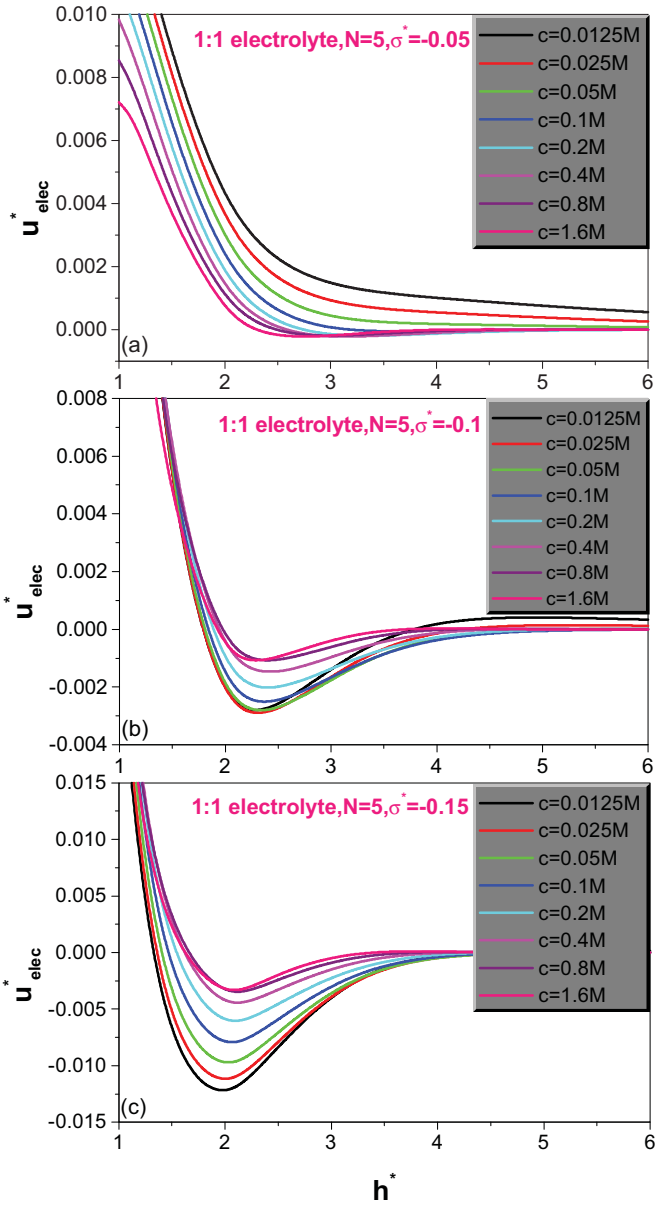

FIG. 5. (Color online) As Fig. 4 but different combinations of site number N of the counterion chain and the surface charge density σ^* are considered.

which lead to the sites being arranged along the rod surfaces. As a result, the mass center of the adsorbed counterion sites is on average farther from the rod surface in the 2:1 electrolyte than in the 1:1 electrolyte, and accordingly h_e^* is larger in the former case than in the latter case. Another problem to be interpreted is the saturation of the LCA-like strength with increasing value of N. Although the increase in N raises the charge magnitude carried by the hydrogen atom, the diameter of the hydrogen ion also increases accordingly; the two factors work in opposite directions, and their combined effect determines the occurrence of the LCA-like strength saturation phenomenon.

When the counterion connectivity is present but N is not large, the chain flexibility is accordingly not large so that h_e^* tends to be large, and this inevitably reduces the

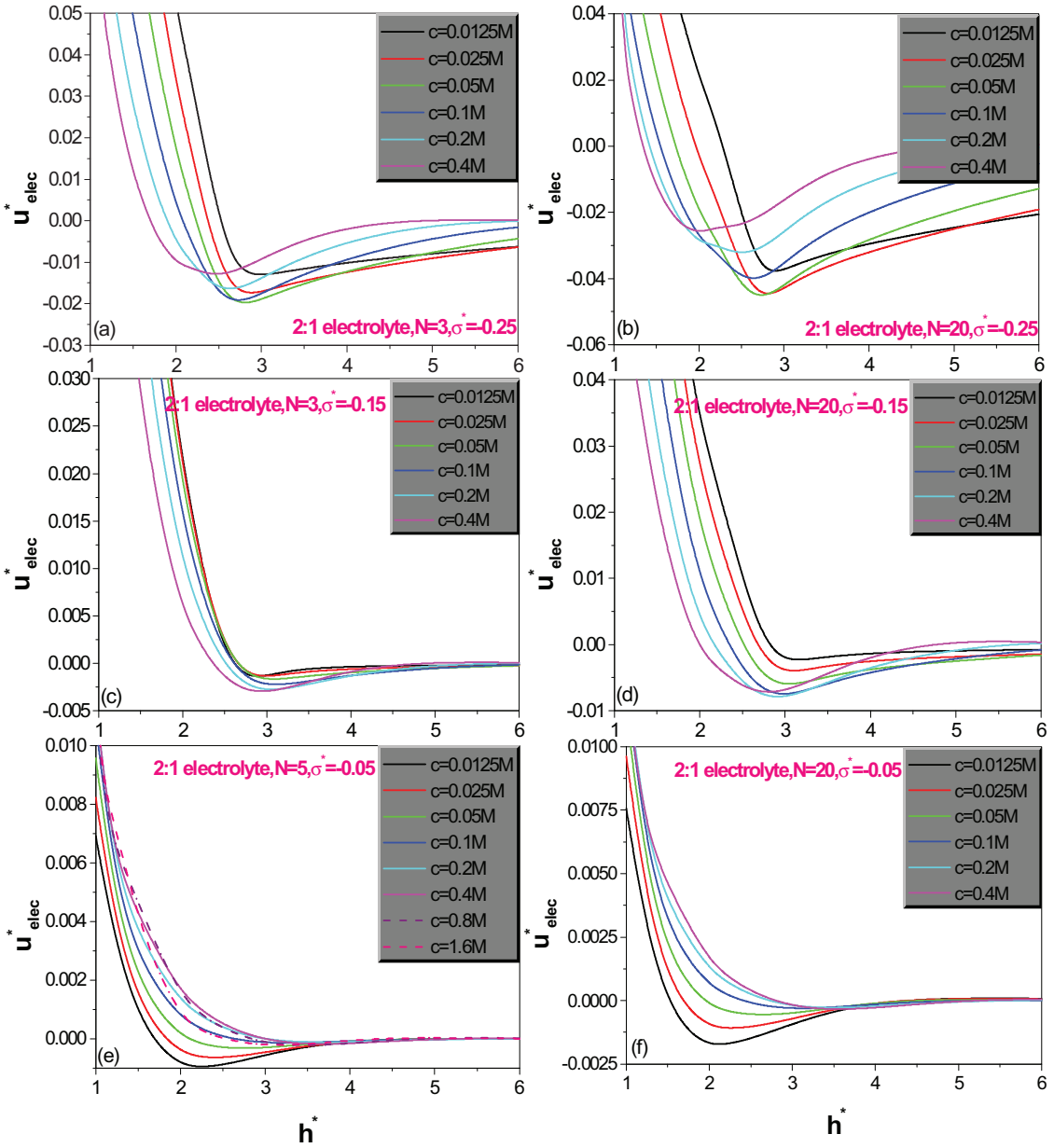

FIG. 6. (Color online) As Fig. 4 except that the 2:1 type electrolyte is considered and the site number $N = 5$ for one case.

hydrogen bond energy; on the other hand, the magnitude of the charges carried by the near surface counterion chain surely rises, as exhibited in Fig. 9 by an obvious increase of ρ_+^* for $N = 3$ in comparison with $N = 1$. The total effect of the above two factors is as illustrated in Fig. 3, which shows that in comparison with the simple electrolyte, the counterion connectivity may raise or reduce the LCA-like strength, and this depends on the site number N considered.

The effects of the electrolyte molar concentration c in different situations are systematically exemplified in Figs. 4–6, which clearly show that the way in which the LCA-like strength changes with c is affected by many factors, such as $|\sigma^*|$, N, and the electrolyte type considered. Figure 4 shows that for a 1:1 type electrolyte the LCA-like strength decreases monotonically with c for the three cases of $|\sigma^*|$ considered if N is large enough; whereas the situation tends to be complex when N is not very large, for example, $N = 3$. To be specific, in the case of $N = 3$, the LCA-like strength indeed decreases monotonically with c if $|\sigma^*|$ is large enough, for example, $\sigma^* = -0.25$; however, the relationship between the LCA-like strength and c can be reversed completely if $|\sigma^*|$ is small enough, for example, $\sigma^* = -0.05$, as shown in Fig. 4(a). There one observes that with the increase of c the LCA-like strength becomes larger or one purely repulsive EPMF tends to weaken and eventually changes from repulsion to attraction. When the value of $|\sigma^*|$ is neither too big nor too small, for example, $|\sigma^*| = 0.15$, the relationship between the LCA-like strength and c becomes nonmonotonic; in the lower-concentration interval the LCA-like strength increases with c, whereas in the higher-concentration interval the relationship is completely reversed, and instead, the LCA-like strength

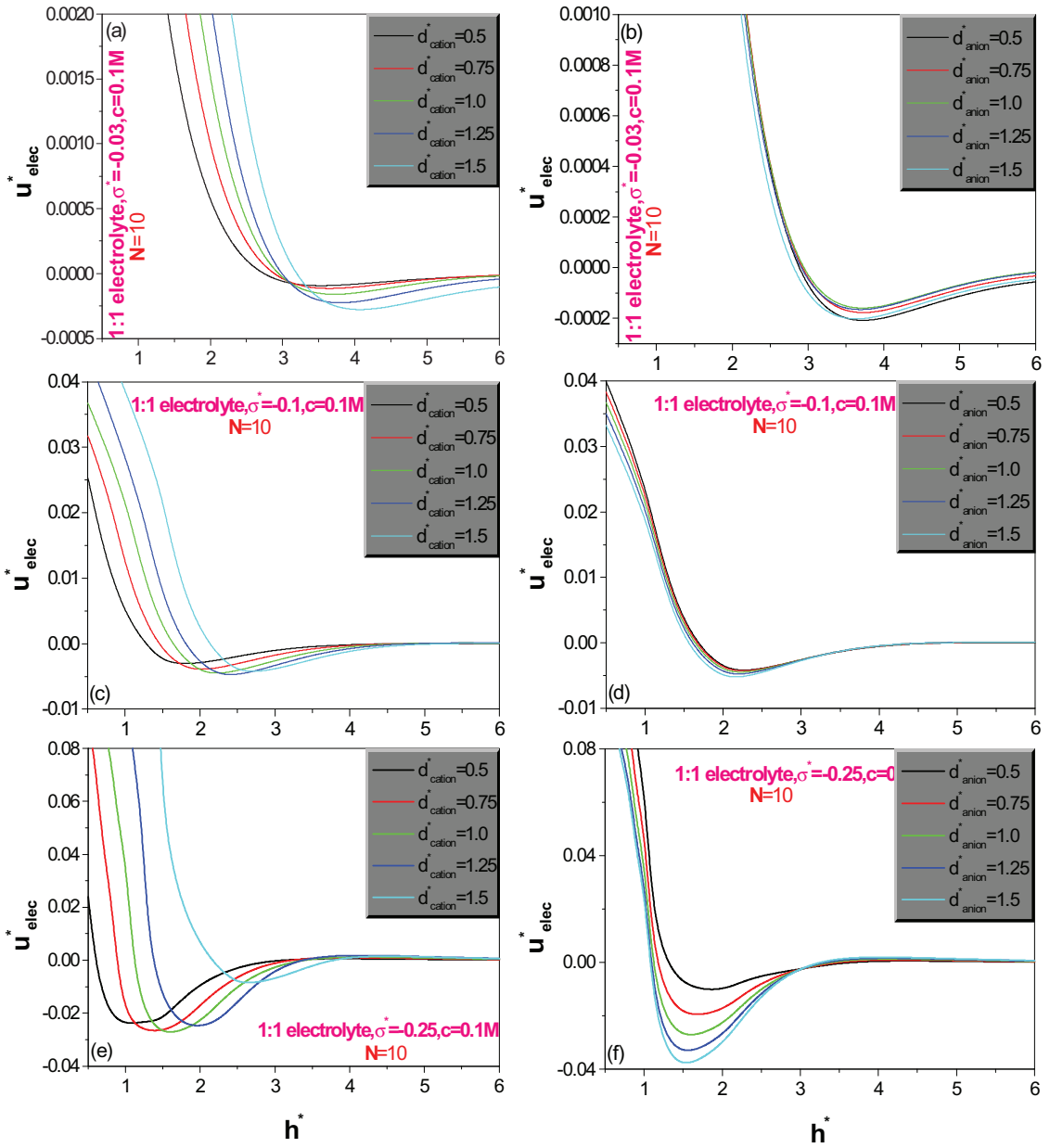

FIG. 7. (Color online) Effects on the EPMF of the counterion site diameter and coion diameter. Values of other solution parameters considered are noted in the figure and described in the text.

decreases with increasing c. If one considers that with the increase of N the chain's flexibility also grows, and this will make it easier for the chain to adjust its configuration to suit adsorption onto the rod surface, the above observations fit in well with the HBSM. According to the HBSM, the relation of the LCA-like strength with c depends on two factors working in opposite directions; one helps in raising the LCA-like strength by more counterion adsorption induced by the enhanced c value, and the other inhibits the increase of the LCA-like strength with c by an electrostatic screening mechanism according to a classical formula for the screening constant $\kappa = (\sum_{i=1}^{N} q_i^2 \rho_i^b / \varepsilon_0 \varepsilon_r k_B T)^{1/2}$ (where ε_0, q_i, and ρ_i^b are the vacuum permittivity, ion charge, and bulk number density, respectively). When $N = 20$ is considered, the strong flexibility of the counterion chain makes its single-layer adsorption capacity reach the relevant saturation value even at the minimum value of the c and $|\sigma^*|$ intervals considered; as a result, only the electrostatic screening effect is at play for all $|\sigma^*|$ cases, and the LCA-like strength of course drops with c, as shown in Figs. 4(b), 4(d), and 4(f). When a shorter chain is considered, like $N = 3$, and at a similar c interval, the lower flexibility of the counterion chain makes its single-layer adsorption capacity reach the relevant saturation value only at the highest $|\sigma^*|$ value considered, and it is far below the adsorption saturation capability at the lowest $|\sigma^*|$ value considered. It is known that according to the HBSM [23,24], when the single-layer adsorption saturation capacity is not reached, the two effects occur in combination, but the electrostatic screening effect is just a secondary consideration; the c-induced adsorption enhancement effect

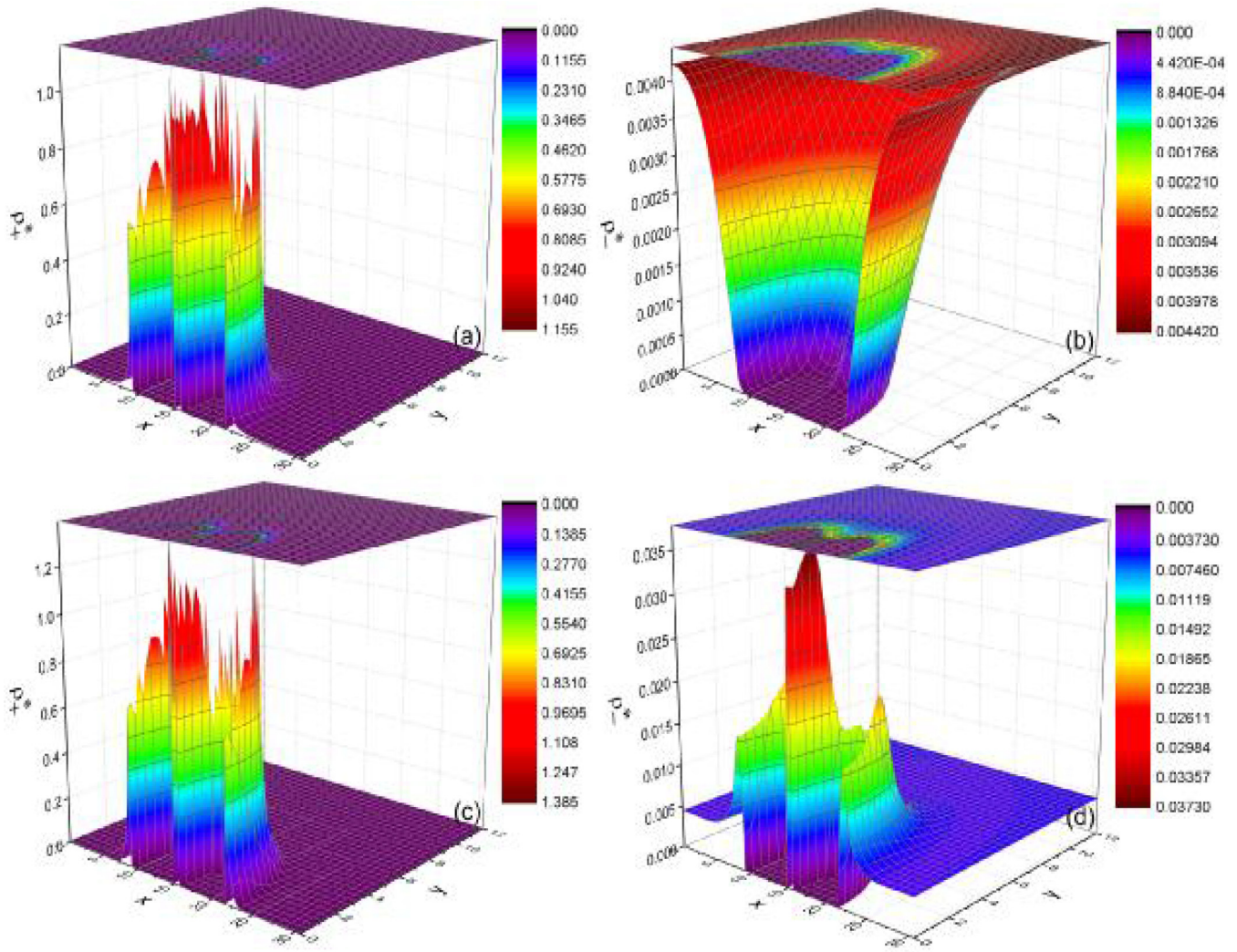

FIG. 8. (Color online) Three-dimensional density profiles of total counterion site and coion. (a),(b) are for the $N = 1$ curve with $h^* = 1.6$, and (c),(d) for the $N = 20$ curve with $h^* = 1.6$ in Fig. 1.

is largely responsible for the final status. As a result, the LCA-like strength is respectively negatively and positively correlated with c at the maximum and minimum of the c interval considered, as shown in Figs. 4(e) and 4(a). On the other hand, when a modest $|\sigma^*|$ is considered, such as $|\sigma^*| = 0.15$, the single-layer adsorption capacity reach its saturation value approximately at $c = 0.1M$; consequently, in the lower concentration interval, approximately from $0.0125M$ to $0.1M$, the correlation between the LCA-like strength and c is positive, whereas in the higher concentration interval, approximately from $0.1M$ to $0.4M$, the correlation becomes negative. The above analysis is supported by the three-dimensional counter- and coion density profiles displayed in Figs. 10 and 11, wherein it is clearly indicated that the maximum counterion density very obviously rises with the bulk molar concentration c when both $|\sigma^*|$ and N are small, whereas it is almost constant with c when both $|\sigma^*|$ and N become larger.

What is displayed in Fig. 5 is similar to what is in the left part of Fig. 4; the main differences between them are the values of the site number N and the surface charge density σ^* as marked therein. One comparison between the two similar figures adds up to one conclusion: that $|\sigma^*|$ at the transformation point in the relation of the LCA-like with c depends on the site number N considered, and decreases with increasing N value. We think that the negative correlation is due to the fact that with the increase of N the enhanced flexibility of the counterion chain means that the single-layer adsorption saturation capacity can be reached more easily, and consequently, for the same concentration interval, $|\sigma^*|$ value smaller by 1 is needed to reach the saturation value. Once the adsorption saturation value is reached, further increase of the c value will no longer raise the LCA-like strength; instead, LCA-like strength–c relation will transform from positive correlation to negative correlation.

Figure 6 describes the relation of the LCA-like strength with c in the 2:1 electrolyte and with $N = 3, 5$ and 20, respectively. The six subfigures lead to the following conclusions for the case of the 2:1 electrolyte: (i) σ^* at the transformation point in the LCA-like-strength–c relation does not depend on the site number N considered, but also differs from those corresponding to the 1:1 electrolyte case; whether $N = 3, 5$ or 20, the LCA-like-strength– c relation displays wholly different

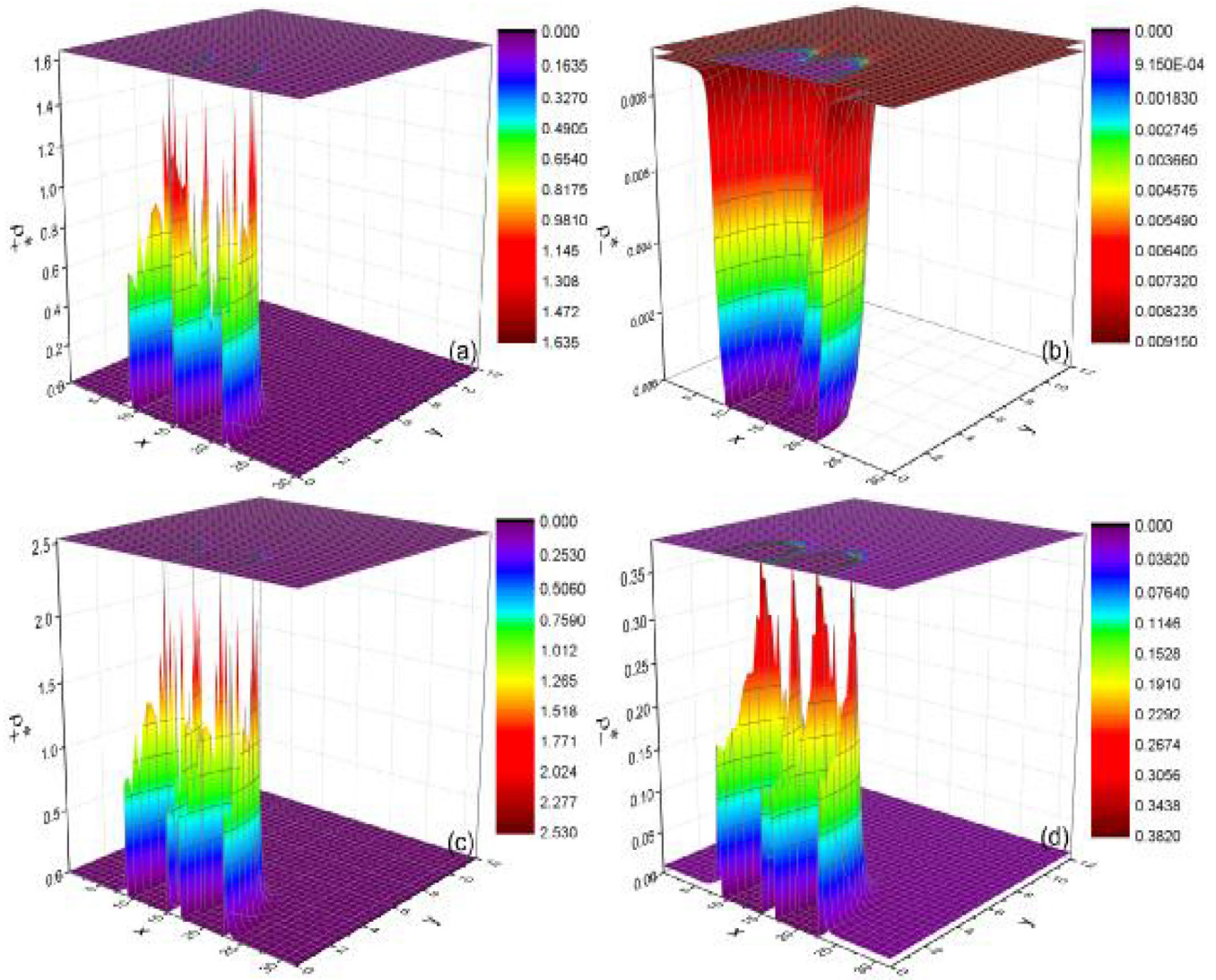

FIG. 9. (Color online) Three-dimensional density profiles of total counterion site and coion. (a),(b) are for the $N = 1$ curve with $h^* = 1.3$, and (c),(d) for the $N = 3$ curve with $h^* = 2.7$, in the Fig. 2, respectively.

characteristics at $\sigma^* = -0.05$ and $\sigma^* = -0.15$, rather than at $\sigma^* = -0.05$ and $\sigma^* = -0.25$, as for the case of the 1:1 electrolyte and $N = 3$. It is of particular interest that the positive and negative correlation relations of LCA-like strength with c in the two cases are diametrically opposed to each other. (ii) At high value of $|\sigma^*|$, the LCA-like-strength–c relation is nonmonotonic, and the LCA-like strengths reach their maximum values at medium concentration; in addition, contrary to the situation of the 1:1 electrolyte wherein h_e^* always decreases with the LCA-like strength, the h_e^*–LCA-like-strength relation offers a nonmonotonic behavior in the case of the 2:1 electrolyte and large $|\sigma^*|$. However, the h_e^*–LCA-like-strength negative correlation relation survives in the low-$|\sigma^*|$ case. The above observations are still understandable from the point of view of chain flexibility. As the counterion site changes from univalence to bivalence, the chain flexibility drops considerably, and by comparison the value of N, another factor influencing the chain flexibility, can no longer play a dominant role; as a result, whether $N = 3$, 5, or 20, the divalent-counterion chain is really less flexible than the univalent-counterion chain. It is easy to imagine that the weakened flexibility is unfavorable for the counterion chain adsorption onto the rod surface unless the adsorption force field, measured by $|\sigma^*|$, is large enough; moreover, given that the value of $|\sigma^*|$ is small, adsorption of the divalent-counterion chain cannot be increased effectively only by increasing the c value. Based on the above analysis, the LCA-like-strength– c negative correlation, diagrammed as in Figs. 6(e) and 6(f), can be understood as a reflection of the dominance of the electrostatic screening due to the considerably reduced flexibility and the small adsorption force field, a combination of which leads to inhibition of the adsorption increase with c even when the single-layer adsorption capacity has not reached its saturation value. On the other hand, an enhanced $|\sigma^*|$ still can overcome the reduced flexibility and help to further the adsorption increase with c; consequently, the saturation adsorption capacity can be reached at $c = 0.05M$, and the LCA-strength–c relationship is nonmonotonic, as shown in Figs. 6(a) and 6(b). When a modest $|\sigma^*|$ value is considered, as in Figs. 6(c) and 6(d), the value of the transformation

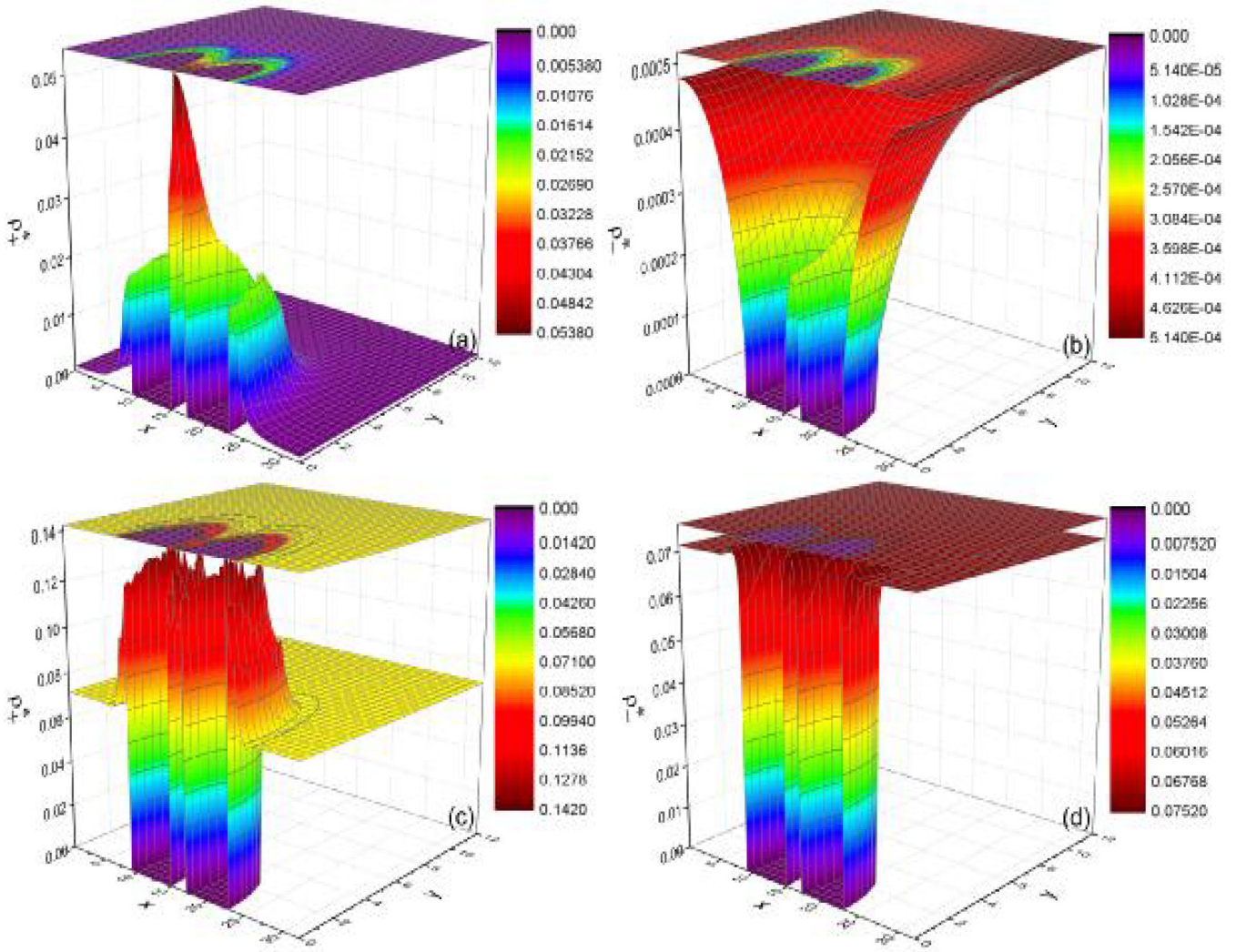

FIG. 10. (Color online) Three-dimensional density profiles of total counterion site and coion. The top and bottom two sub-graphs are for the $c = 0.0125M$ curve with $h^* = 3.0$, and $c = 1.6M$ curve with $h^* = 3.0$, in the top sub-graph of Fig. 3.

concentration c_t at which the single-layer adsorption capacity reaches its saturation value will naturally move to a higher value, for example, $c_t = 0.2M$, in the case of $N = 20$; moreover, in the case of $N = 3$, the c_t value obviously goes beyond the maximum c value considered, and this may be understood as showing that the three site chain is less flexible than the 20- site chain. As regards the strict negative correlation between h_e^* and c, as shown in Figs. 6(a), 6(b), and 6(d), we attribute it to the EDL squeezing effect caused by an enhanced c value. It is known that the c-motivated EDL squeezing effect is common in the simple electrolyte EDL system, one significant feature of which, in comparison with the chain molecule EDL system, is large flexibility. Given that the divalent-cation chain is featured with a considerably reduced flexibility, occurrence of the flexibility-motivated phenomena will definitely be accompanied by certain conditions, which help in weakening the effects caused by small flexibility, such as a high $|\sigma^*|$ value and a high N value, and thus we explain why the strict negative correlation mentioned above occurs only for $|\sigma^*| = 0.25$ or for a lower $|\sigma^*|$ value (like 0.15) but accompanied with a large site number, like $N = 20$.

Figure 7 describes the effects of the counterion site diameter d^*_{cation} and coion diameter d^*_{anion} on the EPMF in a 1:1 electrolyte; and the site number N equals 10, and σ^* is equal to -0.03, -0.1, and -0.25, respectively. It is shown that there are crucial differences between the two effects. First, on the whole, the LCA-like strength increases with d^*_{anion}, and negatively and weakly correlates with the value of h_e^*, as shown in Fig. 7(f). It is generally accepted that the LCA originates from an electrostatic correlation effect, which, according to the language of liquid state theory, actually measures the cross correlation between the electrostatic and steric interactions; on the other hand, as analyzed in literature [23,24], the electrostatic correlation effect will become gradually more noteworthy as the size increases. Consequently, the above-mentioned d^*_{anion} effect is understandable. Moreover, the d^*_{anion} effect becomes increasingly obvious as $|\sigma^*|$ grows steadily and reaches higher values, and this can be explained as an amplification effect of $|\sigma^*|$ on the LCA-like strength. It should be pointed out that d^*_{anion} has little effect on both the LCA-like strength and h_e^* at low values of $|\sigma^*|$, and moreover in the low-$|\sigma^*|$ case, the correlation relationships between the LCA-like

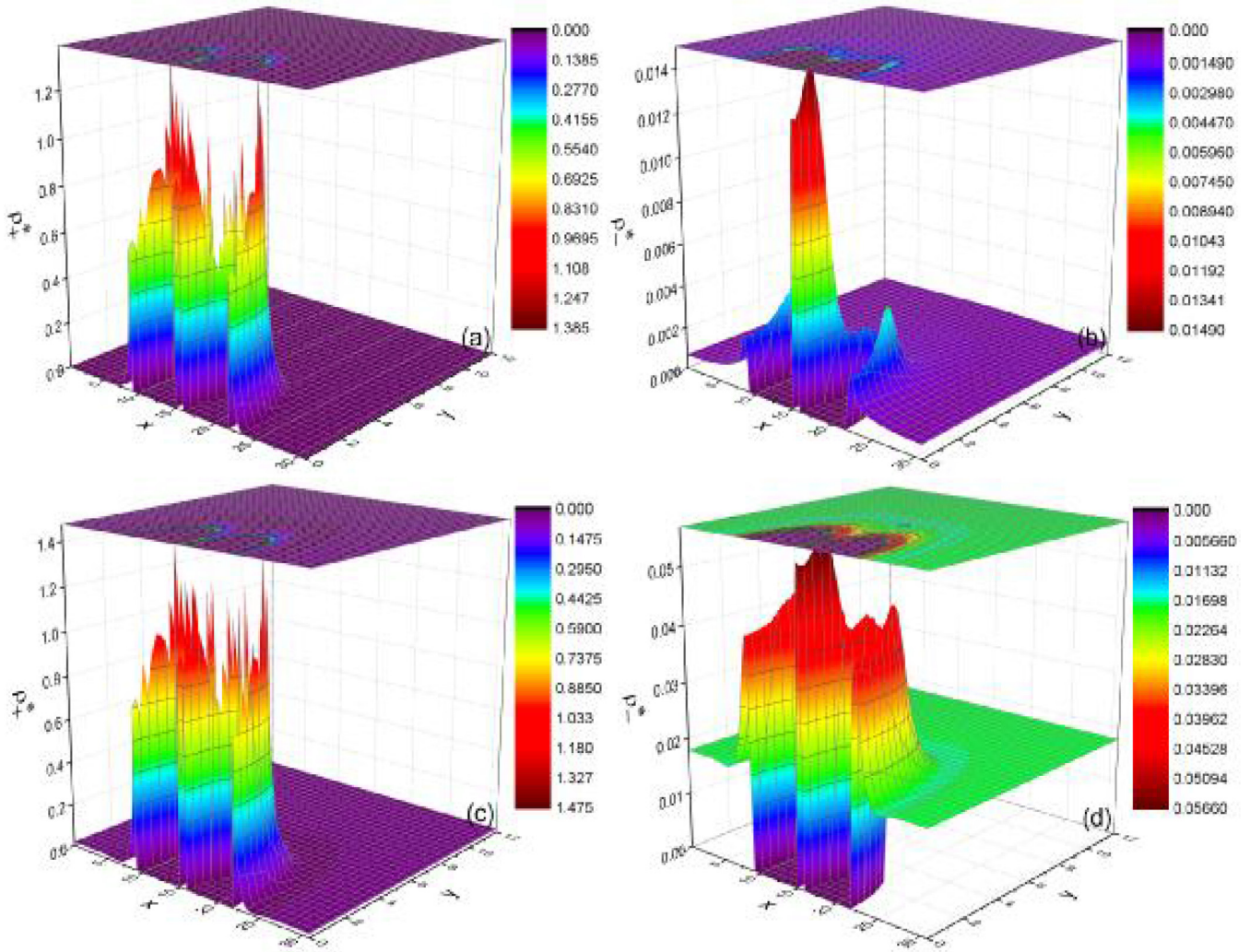

FIG. 11. (Color online) Three-dimensional density profiles of total counterion site and coion. The top and bottom two sub-graphs are for the $c = 0.0125M$ curve with $h^* = 1.8$, and $c = 0.4M$ curve with $h^* = 1.8$, in the lower sub-graph of Fig. 3.

strength and h_e^* and with d_{anion}^* are no longer monotonic. We think this is due to the amplification effect of $|\sigma^*|$ eventually becoming so small that other unknown elements begin to take effect and change the original monotonic relationship. Second, we turn to effect of d_{cation}^*. It is shown in Figs. 7(a), 7(c), and 7(e) that d_{cation}^* has obvious effects on the EPMF for any value of $|\sigma^*|$, and this is reflected in h_e^* and the LCA-like strength. On the one hand, h_e^* always increases monotonically with d_{cation}^*, irrespective of $|\sigma^*|$; on the other hand, the effect on the LCA-like strength turns upon how large $|\sigma^*|$ is, and exhibits an extreme phenomenon at higher values of $|\sigma^*|$ and monotonic change at lower values of $|\sigma^*|$. According to the HBSM, the counterion site serves the role of the hydrogen atom in the hydrogen bonding, and as a result increase of d_{cation}^* necessarily means increase of the length of the hydrogen bond, equivalent to h_e^*, as it is; consequently, the positive correlation between h_e^* and d_{cation}^* is strong evidence for the HBSM. The reason for the extreme phenomenon at higher values of $|\sigma^*|$ is the counterion site single-layer saturation adsorption capacity, which obviously drops with the counterion site size, and whose reduction, in the case of the high-$|\sigma^*|$ zone where the counterion site single-layer adsorption has reached its saturation value, directly diminishes the number of hydrogen bonds likely to be formed. It eventually overwhelms the enhanced electrostatic correlation effects and induces the appearance of an extreme point. However, in the low-$|\sigma^*|$ zone, the counterion site adsorption does not reach the saturation capacity and thus is not affected by the dropping of the saturation capacity. As a result, the enhanced electrostatic correlation effect achieves complete control over the LCA-like strength and induces the monotonic positive correlation between the LCA-like strength and d_{cation}^*.

IV. CONCLUDING REMARKS

To summarize, in the present study, we systematically investigated the influence of the counterion connectivity (i.e., the association of the counterions into a chain molecule) on the EPMF between two similarly charged cylinder rods in a primitive model electrolyte solution; the conclusions reached are summarized as follows.

(1) The counterion connectivity tends to more effectively induce the LCA-like observation even in a one-valence counterion solution wherein the LCA-like effect generally does not occur without the counterion connectivity. For a divalent counterion solution, the counterion connectivity can reinforce or weaken the LCA-like effect depending on the chain length N, and simply increases the equilibrium rod nearest surface separation, wherein the EPMF reaches its minimum, to nearly three times the counterion site diameter, whether N is large or small. If N is large enough, the LCA-like strength tends to be negatively correlated with the electrolyte concentration over the entire range of the rod surface charge magnitude $|\sigma^*|$ considered; whereas if N drops, the correlation tends to become positive with the decrease of the $|\sigma^*|$ value, and particularly for modest $|\sigma^*|$ values, the correlation relationship exhibits an extreme value phenomenon. In the case of a 1:1 electrolyte, the EPMF effects of the diameters of the counterion site and coion are similar in both situations with and without the counterion connectivity.

The present analysis indicates that the mechanism of the LCA-like process in the presence of counterion connectivity is the same as the HBSM [23,24,42], originally proposed for explaining the LCA-like behavior without the counterion connectivity; however, to explain the effect of the counterion chain length N, one has to import the so-called flexibility concept of the counterion chain into the HBSM, and the flexibility of the counterion chain is considered to increase with the chain length N and drop with the counterion site valence. It is noted that the present view that a longer freely and tangentially bonded chain has more flexibility than its shorter chain counterpart is supported by computer simulation reported in the literature [51]. It is clearly indicated in Fig. 3 therein that the critical temperature and critical density of short fully flexible chains formed from tangentially bonded Lennard-Jones monomeric units increases and decreases, respectively, as the number m of the monomers per chain changes from 3, 4, 5, to 6; the change tendencies of the critical parameters are surprisingly similar to those of a spherical model fluid, whose critical temperature and critical density also increases and decreases, respectively, as the potential range increases. Consequently, it is reasonable to coarse-grain the freely and tangentially bonded chain into an atomic fluid modeled by a Lennard-Jones potential with the energy and size parameters increasing as m increases [52]; correspondingly, the critical temperature and critical density, if reduced, respectively, by the energy parameter and size parameter of the monomeric unit, will rise and fall with m, respectively, as shown in Fig. 3 of [51]. Accordingly, the potential range of the effective potential between the coarse-grained "atomic" fluid, if measured by the diameter of the monomeric units, will increase with m; the reason is an enhancement of the flexibility of the chain with m, which brings about more chances of interactions between monomers belonging to two different chains, and consequently, the range of the effective potential rises with m.

(2) The present model is a greatly simplified one due to the adoption of the assumption of surface homogeneities and the continuum solvent model. The surface homogeneities include geometrical homogeneity, which means the colloid surfaces are molecularly smooth and solid, chemical homogeneity, wherein the chemical compositions of the colloid particle are uniformly distributed, and as a result, all differential units of the surface area have equal hydrophobic and hydrophilic properties, and charge homogeneity, which means that the colloid charges are uniformly distributed on the surface. In [42] the present author relieves the charge homogeneity assumption and discloses the obvious influences of the charge discrete distribution on the EPMF in a PM electrolyte solution in the absence of ion connectivity; in [43] the present author investigates the potential of the mean force (PMF) between two face-to-face neutral substrate surfaces patterned with nanoscale corrugations, and illustrates that the resulting changes of the PMF are on the order of the thermal energy. As a result, it will be interesting to study the influences of surface charge discreteness and surface nanoscale corrugations on the EPMF in the presence of ion connectivity. In the present calculations, the differential units of the colloid surface are equally hydrophobic, and neutral interaction between the colloid surface and ion is hard; moreover, the interion neutral interaction is athermal. It will be interesting to study how attractive interactions modify the EPMF. On the other hand, in the present continuum solvent model, the solvent asserts its role only by screening the interion direct electrostatic interaction with a relative permittivity $\varepsilon_r = 78.5$; both the granularity of the solvent and its polarization are completely ignored. It is urgent to extend the continuum solvent model to incorporate more molecular properties of the solvent. Finally, the validity of the HBSM in the presence of all of these complexities is a problem deserving of study.

ACKNOWLEDGMENTS

The author would like to thank three anonymous reviewers for their contributions in helping revise the paper. This project is supported by the National Natural Science Foundation of China (Grants No. 21173271 and No. 21373274).

[1] D. J. Ashton and N. B. Wilding, Quantifying the effects of neglecting many-body interactions in coarse-grained models of complex fluids, Phys. Rev. E **89**, 031301 (2014).

[2] M. Majka and P. F. Gora, Analytical theory of effective interactions in binary colloidal systems of soft particles, Phys. Rev. E **90**, 032303 (2014).

[3] J. McCarty, A. J. Clark, J. Copperman, and M. G. Guenza, An analytical coarse-graining method which preserves the free energy, structural correlations, and thermodynamic state of polymer melts from the atomistic to the mesoscale, J. Chem. Phys. **140**, 204913 (2014).

[4] A. D. Law, L. Harnau, M. Troendle, and S Dietrich, Effective interaction between a colloid and a soft interface near criticality, J. Chem. Phys. **141**, 134704 (2014).

[5] D. Ray, C. Reichhardt, and C. J. O. Reichhardt, Casimir effect in active matter systems, Phys. Rev. E **90**, 013019 (2014).

[6] T. N. Shendruk, M. Bertrand, J. L. Harden, G. W. Slater, and H. W. de Haan, Coarse-grained molecular dynamics simulations of depletion-induced interactions for soft matter systems, J. Chem. Phys. **141**, 244910 (2014).
[7] S. Burger and E. Bartsch, Influence of the polymer size on depletion attraction-induced gel and glass transitions of microgel colloids, Colloids Surf. A **442**, 6 (2014).
[8] H. Q. Wang, C. E. Woodward, and J. Forsman, Exact evaluation of the depletion force between nanospheres in a polydisperse polymer fluid under Theta conditions, J. Chem. Phys. **140**, 194903 (2014).
[9] Y. de Hazan, J. Wilkens-Heinecke, and T. Graule, Modeling the effect of molecular architecture of comb polymers on the behavior of Al_2O_3 dispersions using charge/composition factors (CCF), Colloid Polym. Sci. **292**, 1701 (2014).
[10] F. J. Guzman and J. Y. Walz, Separation of colloidal particles in a packed column using depletion and structural forces, Colloids Surf. A **447**, 131 (2014).
[11] P. M. Lam and Y. A. Zhen, Wormlike chain model of forced desorption of a polymer adsorbed on an attractive wall, J. Stat. Mech.: Theory Exp. (2014) P04020.
[12] B. J. Liu, M. Y. Zhang, C. Zhou, Z. Y. Fu, G. F. Wu, and H. X. Zhang, Hydrophilicity of polymer effects on controlled particle coagulation in batch emulsion polymerization, Colloid Polym. Sci. **292**, 1347 (2014).
[13] S. Tanimura, H. Pathak, and B. E. Wyslouzil, Binary nucleation rates for ethanol/water mixtures in supersonic Laval nozzles: Analyses by the first and second nucleation theorems, J. Chem. Phys. **139**, 174311 (2013).
[14] Z. Konkoli, I. Wegrzyn, and A Jesorka, Forces on an attractive surface generated from a thermoresponsive polymer gel, AIP Adv. **4**, 087137 (2014).
[15] Y. Jiao and P. Akcora, Understanding the role of grafted polystyrene chain conformation in assembly of magnetic nanoparticles, Phys. Rev. E **90**, 042601 (2014).
[16] C. Hanske, C. Schneider, M. Drechsler, A. Wittemann, and A Fery, Salt-regulated attraction and repulsion of spherical polyelectrolyte brushes towards polyelectrolyte multilayers, Phys. Chem. Chem. Phys. **14**, 4196 (2012).
[17] L. Morales-Anda, H. H. Wensink, A. Galindo, and A. Gil-Villegas, Anomalous columnar order of charged colloidal platelets, J. Chem. Phys. **136**, 034901 (2012).
[18] S. Roldan-Vargas, F. Smallenburg, W. Kob, and F Sciortino, Phase diagram of a reentrant gel of patchy particles, J. Chem. Phys. **139**, 244910 (2013).
[19] G. S. Redner, A. Baskaran, and M. F. Hagan, Reentrant phase behavior in active colloids with attraction, Phys. Rev. E **88**, 012305 (2013).
[20] P. Bartlett, L. J. Teece, and M. A. Faers, Sudden collapse of a colloidal gel, Phys. Rev. E **85**, 021404 (2012).
[21] L. Guldbrand, B. Jőnsson, H. Wennerstrőm, and P Linse, Electrical double layer forces. A Monte Carlo study, J. Chem. Phys. **80**, 2221 (1984).
[22] R. Kjellander, S Marčelja, R. M. Pashley, and J. P. A. Quirk, A theoretical and experimental study of forces between charged mica surfaces in aqueous $CaCl_2$ solutions, J. Chem. Phys. **92**, 4399 (1990).
[23] S Zhou, Density functional analysis of like-charged attraction between two similarly charged cylinder polyelectrolytes, Langmuir **29**, 12490 (2013).
[24] S Zhou, Novel anomalies for like-charged attraction between curved surfaces and formulation of a hydrogen bonding style mechanism, AIP Adv. **3**, 032109 (2013) and references therein.
[25] R. Messina, C. Holm, and K Kremer, Strong attraction between charged spheres due to metastable ionized states, Phys. Rev. Lett. **85**, 872 (2000).
[26] D. Frydel and Y. Levin, The double-layer of penetrable ions: An alternative route to charge reversal, J. Chem. Phys. **138**, 174901 (2013), and references therein.
[27] R. Kjellander and S Marčelja, Correlation and image charge effects in electric double layers, Chem. Phys. Lett. **112**, 49 (1984).
[28] R. Kjellander and S Marčelja, Inhomogeneous Coulomb fluids with image interactions between planar surfaces I, J. Chem. Phys. **82**, 2122 (1985).
[29] R. Kjellander, T. Åkesson, B. Jönsson, and S Marčelja, Double layer interactions in mono- and divalent electrolytes: A comparison of the anisotropic HNC theory and Monte Carlo simulations, J. Chem. Phys. **97**, 1424 (1992).
[30] A. G. Moreira and R. R. Netz, Strong-coupling theory for counterion distributions, Europhys. Lett. **52**, 705 (2000).
[31] A. G. Moreira and R. R. Netz, Binding of Similarly Charged Plates with Counterions Only, Phys. Rev. Lett. **87**, 078301 (2001).
[32] R. R. Netz, Electrostatistics of counterions at and between planar charged walls: From Poisson-Boltzmann to the strong-coupling theory, Eur. Phys. J. E **5**, 557 (2001).
[33] P. Kekicheff and O. Spalla, Long-Range Electrostatic Attraction between Similar, Charge-Neutral Walls, Phys. Rev. Lett. **75**, 1851 (1995).
[34] T. Bastug and S Kuyucak, Role of the dielectric constants of membrane proteins and channel water in ion permeation, Biophys. J. **84**, 2871 (2003).
[35] V. S. J. Craig, B. W. Ninham, and R. M. Pashley, The effect of electrolytes on bubble coalescence in water, J. Phys. Chem. **97**, 10192 (1993).
[36] D. Henderson, *Fundamentals of Inhomogeneous Fluids* (Marcel Dekker, New York, 1992).
[37] R. Sundararaman, K. Letchworth-Weaver, and T. A. Arias, A recipe for free-energy functionals of polarizable molecular fluids, J. Chem. Phys. **140**, 144504 (2014).
[38] M. C. Stewart and R. Evans, Layering transitions and solvation forces in an asymmetrically confined fluid, J. Chem. Phys. **140**, 134704 (2014).
[39] D. Gillespie, Restoring the consistency with the contact density theorem of a classical density functional theory of ions at a planar electrical double layer, Phys. Rev. E **90**, 052134 (2014).
[40] K. Yamada, E. Yasuno, Y. Kawabata, T. Okuzono, and T. Kato, Mesoscopic simulation of phase behaviors and structures in an amphiphile-solvent system, Phys. Rev. E **89**, 062310 (2014).
[41] M. Bier and I. Ibagon, Density functional theory of electrowetting, Phys. Rev. E **89**, 042409 (2014).
[42] S Zhou, Effects of discreteness of surface charges on the effective electrostatic interactions, J. Chem. Phys. **140**, 234704 (2014).
[43] S Zhou, Effects of nanoscale surface corrugation on surface-to-surface effective potential, Microfluid. Nanofluid. **14**, 859 (2013).

[44] S. Zhou, S. Lamperski, and M. Zydorczak, Properties of a planar electric double layer under extreme conditions investigated by classical density functional theory and Monte Carlo simulations, J. Chem. Phys. **141**, 064701 (2014).

[45] S. Jain, A. Dominik, and W. G. Chapman, Modified interfacial statistical associating fluid theory: A perturbation density functional theory for inhomogeneous complex fluids, J. Chem. Phys. **127**, 244904 (2007).

[46] S. Zhou, Enhanced KR-fundamental measure functional for inhomogeneous binary and ternary hard sphere mixtures, Commun. Theor. Phys. **55**, 46 (2011).

[47] H. Hansen-Goos and R. Roth, A new generalization of the Carnahan-Sterling equation of state to additive mixtures of hard spheres, J. Chem. Phys. **124**, 154506 (2006).

[48] E. Kierlik and M. L. Rosinberg, Free-energy density functional for the inhomogeneous hard-sphere fluid: Application to interfacial adsorption, Phys. Rev. A **42**, 3382 (1990).

[49] Y Rosenfeld, Free-Energy Model for the Inhomogeneous Hard-Sphere Fluid Mixture and Density-Functional Theory of Freezing, Phys. Rev. Lett. **63**, 980 (1989).

[50] L Blum, Mean spherical model for asymmetric electrolytes I. Method of solution, Mol. Phys. **30**, 1529 (1975); K. Hiroike, Supplement to Blum's theory for asymmetric electrolytes, *ibid.* **33**, 1195 (1977).

[51] F. J. Blas, A. I. Moreno-Ventas Bravo, J. Algaba, F. J. Martínez-Ruiz, and L. G. MacDowell, Effect of molecular flexibility of Lennard-Jones chains on vapor-liquid interfacial properties, J. Chem. Phys. **140**, 114705 (2014).

[52] J. O. Hirschfelder, C. F. Curtiss, and R. B. Bird, *Molecular Theory of Gases and Liquids* (Wiley, New York, 1954).